Contribution from the Chemistry Department and Biophysics Program,
University of Virginia, Charlottesville, Virginia 22901

Chiral Recognition between Dissymmetric $Ln(dpa)_3^{3-}$ and Co(III)–Nucleotide Complexes in Aqueous Solution. Enantioselective Luminescence Quenching as a Probe of Intermolecular Chiral Discrimination

David H. Metcalf,*,† John M. McD. Stewart,† Seth W. Snyder,‡ Charles M. Grisham,†
and F. S. Richardson*,†

Received November 7, 1991

Time-resolved chiroptical luminescence spectroscopy is used to investigate enantioselective excited-state quenching processes in solution samples that contain a racemic mixture of chiral luminophores and a small concentration of dissymmetric quencher molecules. The luminophores are $Ln(dpa)_3^{3-}$ complexes (Ln ≡ Eu^{3+} or Tb^{3+}, dpa ≡ a dipicolinate dianion) that have tris(terdentate) chelate structures of D_3 symmetry with either left-handed (Λ) or right-handed (Δ) configurational chirality about the trigonal axis. The quenchers are 6-coordinate Co(III) complexes with the general stoichiometric formula $Co(NH_3)_4$(ndp) *or* $Co(NH_3)_4$(ntp), where ndp denotes a *diphosphate* nucleotide ligand and ntp denotes a *triphosphate* nucleotide ligand. In these complexes the nucleotide ligand is coordinated to Co(III) via bidentate chelation in which the donor moieties are oxygen atoms from adjacent phosphate groups (β, α in ndp and γ, β in ntp nucleotides). The nucleotides used as ligands in this study are the following: adenosine diphosphate and triphosphate (adp and atp), guanosine diphosphate and triphosphate (gdp and gtp), inosine diphosphate and triphosphate (idp and itp), cytidine triphosphate (ctp), uridine triphosphate (utp), and deoxythymidine triphosphate (ttp). The $Co(NH_3)_4$(nucleotide) complexes have dissymmetric structures both within and external to the $Co(NH_3)_4$(phosphate) coordination unit, but under the conditions employed in this study, they exist as mixtures of diastereomers that are quasi-racemic with respect to chirality *within* the $Co(NH_3)_4$(phosphate) coordination units. All of the $Co(NH_3)_4$(ndp) and $Co(NH_3)_4$(ntp) complexes (denoted hereafter by CoNDP and CoNTP, respectively) perform as quenchers of $Eu(dpa)_3^{3-}$ (Eu*) and $Tb(dpa)_3^{3-}$ (Tb*) luminescence, and the quenching rate constants exhibit significant variations among the different systems. For Eu* quenching, the rate constants vary from 2.2×10^6 to 16.9×10^6 M^{-1} s^{-1}, and for Tb* quenching, the rate constants vary from 4.3×10^6 to 14.4×10^6 M^{-1} s^{-1}. Additionally, all of the CoNDP and CoNTP complexes exhibit *enantiodifferential* quenching of ΛLn* vs ΔLn* enantiomers (of the $Eu(dpa)_3^{3-}$ and $Tb(dpa)_3^{3-}$ luminophores), and the differential rate parameters associated with this quenching reveal striking variations in both the *degree* and *sense* of enantiomeric preference shown by the various quencher complexes. CoATP shows an enantiomeric preference that is the same as that shown by CoCTP, CoUTP, and CoTTP, but is opposite that of CoGTP, CoITP, CoGDP, CoIDP, and CoADP. Furthermore, whereas CoATP shows a 32% greater preference for one Tb* enantiomer over the other, CoADP shows only a 1% preference (for the *opposite* enantiomer). All of the CoNDP and CoNTP complexes have the same $Co(NH_3)_4$(phosphate) coordination unit, and the observed variations in the quenching properties (*within* either the CoNDP or CoNTP series) must be attributed to structural differences between their nucleoside base moieties. The quenching properties and their variations are discussed within the context of a model in which it is assumed that quenching occurs via Ln*-to-Co electronic energy-transfer processes in transient *contact* encounters between the luminophore and quencher species in solution.

Introduction

Recently we reported luminescence quenching measurements that probe enantioselective interactions between dissymmetric metal complexes in aqueous solution.[1-4] The measurements were carried out on samples that contained a racemic mixture of dissymmetric tris(terdentate) lanthanide(III) complexes in solution with a *resolved* (or *partially resolved*) concentration of dissymmetric tris(bidentate) transition-metal complexes. The lanthanide complexes contained either Eu(III) or Tb(III), and luminescence from these complexes was excited with unpolarized light at a wavelength corresponding to an absorptive transition of the Ln(III) species. The transition-metal complexes contained either Co(III) or Ru(II), and they functioned as quenchers of the Ln(III) luminescence. The ligands and net charges on both the lanthanide (luminophore) and transition-metal (quencher) complexes were varied, but *all* of the complexes had equilibrium structures of either D_3 or pseudo-D_3 (actual C_2) symmetry, and these structures could be classified as having either left-handed (Λ) or right-handed (Δ) configurational chirality about the metal center of the complex. Unpolarized excitation of the racemic lanthanide complexes produces an initially racemic excited-state population of ΛLn* and ΔLn* enantiomers, but this population may evolve to a nonracemic composition if the resolved (or partially resolved) transition-metal complexes differentially quench the ΛLn* and ΔLn* enantiomers. In our experiments, generation of enantiomeric excess in the Ln* excited-state population was monitored by chiroptical luminescence measurements, and the data obtained from these measurements were used to characterize *enantioselectivity* in the quenching of ΛLn* vs ΔLn* enantiomers by the chiral transition-metal complexes. The use of pulsed excitation and time-resolved chiroptical measurements permitted the direct determination of differential rate parameters associated with *homochiral* (ΛLn*–ΛQ or ΔLn*–ΔQ) vs *heterochiral* (ΛLn*–ΔQ or ΔLn*–ΛQ) quenching actions, and those rate parameters were related to chiral discriminatory interactions between the excited lanthanide complexes (Ln*) and the transition-metal quencher (Q) complexes.

In the luminophore (Ln*)–quencher (Q) systems examined in the studies cited above, quenching of Ln* luminescence occurs via an electronic energy-transfer mechanism dominated by Ln* (donor)–Q (acceptor) electron-exchange interactions within short-lived collisional complexes.[2] Quenching efficiency *and* enantioselectivity exhibited sensitivity to both the electronic and stereochemical properties of the constituent Ln* and Q members of the donor–acceptor pairs, and in several systems, heterochiral vs homochiral quenching rates differed by a factor of 2 or more.[3,5] The magnitude and variability of the enantioselectivity observed in these quenching studies indicated that enantioselective quenching measurements can provide a very sensitive means for investigating intermolecular chiral recognition/discrimination phenomena. Furthermore, it was shown that these measurements may also be used to determine the enantiomeric composition (or optical purity) of partially resolved quencher samples.[3,5]

* Authors to whom correspondence should be addressed.
† Chemistry Department.
‡ Biophysics Program. Present address: Argonne National Laboratory, Argonne, IL 60439.

(1) Metcalf, D. H.; Snyder, S. W.; Wu, S.; Hilmes, G. L.; Riehl, J. P.; Demas, J. N.; Richardson, F. S. *J. Am. Chem. Soc.* **1989**, *111*, 3082–3083.
(2) Metcalf, D. H.; Snyder, S. W.; Demas, J. N.; Richardson, F. S. *J. Am. Chem. Soc.* **1990**, *112*, 5681–5695.
(3) Metcalf, D. H.; Snyder, S. W.; Demas, J. N.; Richardson, F. S. *J. Phys. Chem.* **1990**, *94*, 7143–7153.
(4) Richardson, F. S.; Metcalf, D. H.; Glover, D. P. *J. Phys. Chem.* **1991**, *95*, 6249–6259.
(5) Snyder, S. W. Ph.D. Dissertation, University of Virginia, 1989.

0020-1669/92/1331-2445$03.00/0

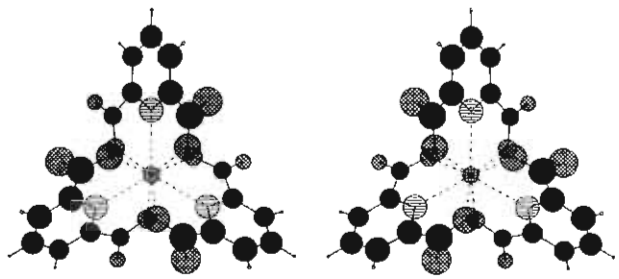

Λ–Ln(dpa)$_3^{3-}$ Δ–Ln(dpa)$_3^{3-}$

Figure 1. Structural representations of both enantiomers of the Ln(dpa)$_3^{3-}$ complex, viewed down the trigonal (C_3) axis. Atom types: ● ≡ metal atom, ● ≡ nitrogen atom, ● ≡ oxygen atom, ● ≡ carbon atom, ○ ≡ hydrogen atom.

In the study reported here, we investigated enantioselective quenching of Ln(dpa)$_3^{3-}$ luminescence by Co(III) complexes that contain four NH_3 ligands and one nucleotide ligand. The Ln(dpa)$_3^{3-}$ complexes have tris(terdentate) structures in which each dpa (dipicolinate) ligand is coordinated to the lanthanide ion (Ln ≡ Eu^{3+} or Tb^{3+}) via two carboxylate oxygen atoms and a pyridyl nitrogen atom. The bicyclic chelate systems formed by the dpa ligands are planar, and they are arranged in a helical (three-bladed propeller) configuration about the trigonal symmetry axis of the complex (which has D_3 point-group symmetry).[6] The Ln(dpa)$_3^{3-}$ complexes may be formed in neutral aqueous solution from stoichiometric amounts of Ln^{3+} and dpa, and under these conditions they exist as a racemic mixture of left-handed (Λ) and right-handed (Δ) configurational isomers (i.e., enantiomers). Structural representations of both enantiomers of the Ln(dpa)$_3^{3-}$ complex are shown in Figure 1. Both Eu(dpa)$_3^{3-}$ and Tb(dpa)$_3^{3-}$ have been used as luminescent probes in our previous studies of enantioselective excited-state quenching kinetics, and their relevant chiroptical properties are described in refs 2 and 7.

The dissymmetric Co(III) complexes employed as quenchers in our previous studies had tris(bidentate) chelate structures that could be chemically resolved and isolated as pure optical isomers. The resolved enantiomers of these complexes had rigid and well-defined stereochemical structures (of known absolute configuration about the metal ion), and they exhibited strong circular dichroism in the d–d electronic transitions of Co(III). The complexes were made from neutral ligands, and they could be assigned a formal charge of $ze = +3e$. These complexes differ significantly from the Co(NH$_3$)$_4$(nucleotide) complexes investigated in the present study, particularly with respect to net charge, stereochemical structure, and sources of structural chirality. Both triphosphate and diphosphate nucleotides of adenosine, guanosine, and inosine are represented in our studies, as well as the triphosphate nucleotides of cytidine, uridine, and deoxythymidine. In each case the nucleotide ligand is coordinated to Co(III) via *bidentate* chelation in which the donor moieties are oxygen atoms from adjacent phosphate groups (γ, β in the triphosphate and β, α in the diphosphate nucleotides). Hereafter, we shall denote the tri- and diphosphate nucleotide ligands by ntp and ndp, respectively, where n identifies the nucleoside component (n ≡ a for adenosine, g for guanosine, i for inosine, u for uridine, c for cytidine, and t for thymidine). The Co(NH$_3$)$_4$(ntp) complexes have a net negative charge in neutral aqueous solution, whereas the Co(NH$_3$)$_4$(ndp) complexes are formally uncharged. Both types of complexes are substitutionally inert (and constitutively nonlabile) in neutral aqueous solution, but the noncoordinated parts of the nucleotide ligand may exhibit stereochemical diversity and lability.

Nucleotide complexes of cobalt(III) ammines were first prepared and characterized by Cleland and co-workers,[8,9] with special emphasis on Co(NH$_3$)$_4$(atp) and Co(NH$_3$)$_4$(adp). In examining the chiroptical properties of these systems, attention was focused on chirality associated with the asymmetric phosphorus atom in the six-membered chelate ring of the γ,β*-bidentate atp complex and the β,α*-bidentate adp complex (asterisk identifies location of the asymmetric phosphorus atom).[8c,9] The asymmetric phosphorus atom has two exocyclic substituents—an oxygen atom and adenosine monophosphate (amp), and permutation of these two substituents generates two stereoisomers that differ with respect to their configurational chirality about the asymmetric phosphorus atom. These two isomers have been labeled Λ and Δ by Cleland and co-workers,[8c,9] but it must be kept in mind that they represent *diastereomers* (not enantiomers) of the overall Co(NH$_3$)$_4$(nucleotide) structures because the nucleoside moiety also contains chiral centers (asymmetric carbon atoms in the ribosyl group). If the nucleoside moiety is removed from a Co(NH$_3$)$_4$(ntp) complex, the Λ and Δ isomers of the resultant Co(NH$_3$)$_4$(ppp) complex (where ppp denotes a bidentate tripolyphosphate ligand) are enantiomers.

Cornelius and Cleland[8c] have reported circular dichroism (CD) spectra of partially separated Λ and Δ diastereomers of Co(NH$_3$)$_4$(atp) and of Co(NH$_3$)$_4$(adp), and they have also reported CD spectra of partially resolved Λ and Δ enantiomers of Co(NH$_3$)$_4$(ppp). Positive-signed CD in the 500–600-nm spectral region of each complex was correlated with Λ isomers, and negative-signed CD was correlated with Δ isomers. Unresolved mixtures of the Λ and Δ diastereomers of Co(NH$_3$)$_4$(atp) showed only a very weak CD in the 500–600-nm region, with both positive and negative components of approximately equal intensity. Optical absorption in the 500–600-nm spectral region can be assigned to d–d transitions of Co(III), and the CD results obtained for Co(NH$_3$)$_4$(atp) indicate that the *d–d* optical activity is determined almost entirely by the configurational chirality at the asymmetric phosphorus atom of the Co–atp chelate ring. It appears that the d electrons of Co(III) essentially view the Λ and Δ diastereomers as enantiomers, and they are relatively insensitive to the details of chiral structure associated with the nucleoside moiety of the complex. Cornelius and Cleland[8c] also showed that configurational chirality at the asymmetric phosphorus atom plays a crucial *stereoselective* role in the yeast hexokinase catalyzed reaction: [Co(NH$_3$)$_4$(atp)]$^-$ + glucose ↔ [Co(NH$_3$)$_4$(glucose-6-P)(adp)]$^{2-}$ + H^+. Only the Λ diastereomer of Co(NH$_3$)$_4$(atp) performs as an active substrate in this enzyme-catalyzed reaction, which indicates a high degree of chiral discrimination in the interactions between hexokinase and the Λ vs Δ diastereomers of Co(NH$_3$)$_4$(atp).

In the present study, we examine enantioselective luminescence quenching results obtained for samples that contain *racemic* Eu(dpa)$_3^{3-}$ *or* Tb(dpa)$_3^{3-}$ (the luminophores) in aqueous solution with *unresolved mixtures* of Λ and Δ diastereomers of Co(NH$_3$)$_4$(ntp) or Co(NH$_3$)$_4$(ndp) complexes (the quenchers). Enantioselective quenching in these luminophore–quencher systems reflects intermolecular chiral discrimination that depends on the details of chiral structure associated with the nucleoside moiety of the Co(III) complexes. The quenching mechanism involves electronic energy transfer from $4f^N$ donor states of the lanthanide ion to $3d^6$ acceptor states of Co(III), and it is reasonable to assume that this energy transfer occurs via short-range intermolecular interactions (e.g., electron-exchange interactions in luminophore–quencher "collisional" complexes).[2] Enantioselectivity in the quenching may reflect nucleoside-dependent chirality in the $3d^6$ electronic-state structure of Co(III) *and/or* nucleoside-dependent stereochemical structure in the luminophore–quencher collisional complexes. However, we have already noted that the chiroptical properties reported for Co(NH$_3$)$_4$(atp) suggest very

(6) (a) Albertsson, J. *Acta Chem. Scand.* **1972**, *26*, 985–1004. (b) Albertsson, J. *Acta Chem. Scand.* **1972**, *26*, 1005–1017.
(7) Metcalf, D. H.; Snyder, S. W.; Demas, J. N.; Richardson, F. S. *J. Am. Chem. Soc.* **1990**, *112*, 469–479.
(8) (a) Cornelius, R. D.; Hart, P. A.; Cleland, W. W. *Inorg. Chem.* **1977**, *16*, 2799–2805. (b) Merritt, E. A.; Sundaralingam, M.; Cornelius, R. D.; Cleland, W. W. *Biochemistry* **1978**, *17*, 3274–3278. (c) Cornelius, R. D.; Cleland, W. W. *Biochemistry* **1978**, *17*, 3279–3286.
(9) Cleland, W. W.; Mildvan, A. S. In *Advances in Inorganic Biochemistry*; Eichen G., Marzilli, L., Eds.; Elsevier/North Holland: New York, 1979; Chapter 6, pp 163–191.

weak chirality-dependent interactions between the 3d electrons of Co(III) and structure within the nucleoside moiety.[8c,9] Therefore, it is likely that enantioselective quenching observed for the $Ln(dpa)_3^{3-}$–$Co(NH_3)_4$(nucleotide) systems can be attributed to nucleoside-controlled stereoselectivity in the formation and structure of luminophore–quencher collisional complexes.

Theory and Measurement Methodology

The general theory and measurement methodologies employed in enantioselective luminescence quenching studies have been described previously.[2,4] Here we shall summarize and briefly discuss only those aspects of theory and methodology that are directly relevant to the experiments reported in the present paper. In these experiments, the luminophores are $Ln(dpa)_3^{3-}$ complexes (where Ln ≡ Eu^{3+} or Tb^{3+}), and the quenching species are either $Co(NH_3)_4$(ntp) or $Co(NH_3)_4$(ndp) complexes (as described in the Introduction). The experiments were carried out on neutral aqueous (H_2O or D_2O) solution samples (at 4 and 20 °C) that contained 100 μM phosphate buffer, a luminophore concentration of 10 mM, and a quencher concentration of 50 μM for the diphosphate nucleotides and 100 μM for the triphosphate nucleotides. The luminophore concentration was a *racemic* mixture of Λ-$Ln(dpa)_3^{3-}$ and Δ-$Ln(dpa)_3^{3-}$ *enantiomers* (denoted hereafter by ΛLn and ΔLn for ground-state populations, and by ΛLn* and ΔLn* for excited-state populations). The quencher concentration contained an unresolved mixture of $Co(NH_3)_4$(nucleotide) diastereomers that has approximately equimolar amounts of isomers that are distinguished by configurational chirality at the asymmetric phosphorus atom of the Co–nucleotide chelate ring. As was noted earlier (see Introduction), Cleland and co-workers[8c,9] labeled these two types of diastereomers as Λ and Δ, and they correlated the Λ isomers of $Co(NH_3)_4$(atp) with an *R* absolute configuration at the asymmetric phosphorus atom and the Δ isomers with an *S* absolute configuration (where the *R* and *S* labels for absolute configuration conform to the Cahn–Ingold–Prelog conventions).[10] In the following discussion, we shall find it convenient to use *R* and *S* labels (rather than Cleland's Λ and Δ) for diastereomers of the cobalt complexes, and we shall represent the total quencher (Q) concentration in our samples as a sum of RQ and SQ concentrations.

In our experiments, the racemic $Ln(dpa)_3^{3-}$ complexes (*rac*-Ln) are excited with a pulse of *unpolarized* light to produce an initially racemic excited-state population (*rac*-Ln*). Generation of enantiomeric excess in this Ln* population (via enantioselective excited-state quenching processes) is then monitored by chiroptical luminescence measurements. In these measurements, the sums and differences of *left*- and *right*-circularly polarized luminescence intensities are determined, and the ratios of these sums and differences are correlated with enantiomeric excess produced in the Ln* population by enantioselective quenching. The experimentally measured quantities are

$$I(\lambda',t) = I_L(\lambda',t) + I_R(\lambda',t) \quad (1)$$

$$\Delta I(\lambda',t) = I_L(\lambda',t) - I_R(\lambda',t) \quad (2)$$

$$g_{em}(\lambda',t) = 2\Delta I(\lambda',t)/I(\lambda',t) \quad (3)$$

where $I_L(\lambda',t)$ and $I_R(\lambda',t)$ denote intensities for the *left*- and *right*-circularly polarized components of the sample luminescence at the emission wavelength λ′ and at time *t* after excitation. Following previous practice, we refer to *I* as a *total luminescence* (TL) intensity, we refer to ΔI as a *circularly polarized luminescence* (CPL) intensity, as we call g_{em} an *emission dissymmetry factor*.[11] The relationship between $g_{em}(\lambda',t)$ and enantiomeric excess in the Ln* emitting-state population is

$$g_{em}(\lambda',t) = \eta^t_{Ln^*} g^{\Lambda}_{em}(\lambda') \quad (4)$$

where $g^{\Lambda}_{em}(\lambda')$ denotes an intrinsic emission dissymmetry factor for *pure* ΛLn* enantiomers at wavelength λ′ and $\eta^t_{Ln^*}$ denotes a time-dependent enantiomeric excess defined by

$$\eta^t_{Ln^*} = \frac{[\Lambda Ln^*]^t - [\Delta Ln^*]^t}{[\Lambda Ln^*]^t + [\Delta Ln^*]^t} = \frac{[\Lambda Ln^*]^t - [\Delta Ln^*]^t}{[Ln^*]^t} \quad (5)$$

where $[\Lambda Ln^*]^t$ etc. represent time-dependent concentrations of emitting species. Information about the kinetics of enantioselective excited-state quenching is contained in $\eta^t_{Ln^*}$.

Kinetic Model and Rate Expressions. The kinetic model used for the present luminophore–quencher systems differs from that presented previously[2,4] in that the quencher complexes are now diastereomers rather than the enantiomeric transition-metal complexes investigated previously. The RQ and SQ nucleotide complexes are not optical antipodes, and so the number of quenching rate constants cannot be reduced to the two (homochiral and heterochiral) quenching rate constants as in previous work. For the luminophore–quencher systems examined in this study, the following processes are considered:

(a) excitation of *rac*-Ln with unpolarized light

$$\Lambda Ln + h\nu \rightarrow \Lambda Ln^* \qquad k^{\Lambda}_{exc}$$

$$\Delta Ln + h\nu \rightarrow \Delta Ln^* \qquad k^{\Delta}_{exc}$$

(b) decay of Ln* complexes in the absence of quencher (Q) actions

$$\Lambda Ln^* \rightarrow \Lambda Ln + h\nu' + \text{nonradiative energy} \qquad k^{\Lambda}_0$$

$$\Delta Ln^* \rightarrow \Delta Ln + h\nu' + \text{nonradiative energy} \qquad k^{\Delta}_0$$

(c) de-excitation of Ln* complexes by quencher species

$$\Lambda Ln^* + RQ \rightarrow \Lambda Ln + RQ^* \qquad k^{\Lambda R}_q$$

$$\Lambda Ln^* + SQ \rightarrow \Lambda Ln + SQ^* \qquad k^{\Lambda S}_q$$

$$\Delta Ln^* + RQ \rightarrow \Delta Ln + RQ^* \qquad k^{\Delta R}_q$$

$$\Delta Ln^* + SQ \rightarrow \Delta Ln + SQ^* \qquad k^{\Delta S}_q$$

(d) interconversions of ΛLn* and ΔLn* enantiomers

$$\Lambda Ln^* \rightarrow \Delta Ln^* \qquad k^{\Lambda}_{conv}$$

$$\Delta Ln^* \rightarrow \Lambda Ln^* \qquad k^{\Delta}_{conv}$$

Among the 10 rate constants shown above, there are three pairwise identities, and the number of unique rate constants can be reduced to seven: $k_{exc} \equiv k^{\Lambda}_{exc} = k^{\Delta}_{exc}$; $k_0 \equiv k^{\Lambda}_0 = k^{\Delta}_0$; $k^{\Lambda R}_q$; $k^{\Lambda S}_q$; $k^{\Delta R}_q$; $k^{\Delta S}_q$; and $k_{conv} \equiv k^{\Lambda}_{conv} = k^{\Delta}_{conv}$. The processes shown in (d) reflect enantiomer interconversions that might occur in the stereochemically labile Ln* systems, and if k_{conv} and k_0 are of comparable magnitude, these processes can effectively "undo" any enantiomeric resolution produced in the quenching processes. In previous studies, we have shown that the ratio of k_{conv} to k_0 is less than 0.1 for $Ln(dpa)_3^{3-}$ complexes in aqueous solution at temperatures below 315 K, and at 293.2 K this ratio is ca. 0.03.[5,7] All of the measurements reported in the present study were carried out on samples at 293.2 or 277.3 K, and hereafter we shall assume that ΛLn* ↔ ΔLn* enantiomer interconversion processes are unimportant in our analyses of chiroptical luminescence data.

The rate laws of interest are those showing the rates at which the ΛLn* and ΔLn* excited-state populations decay after their preparation with a pulse of unpolarized light. If we neglect ΛLn* ↔ ΔLn* interconversion processes (vide supra), the appropriate differential rate expressions may be written as

$$\frac{-d[\Lambda Ln^*]}{dt} = (k_0 + k^{\Lambda R}_q[RQ] + k^{\Lambda S}_q[SQ])[\Lambda Ln^*] \quad (6)$$

$$\frac{-d[\Delta Ln^*]}{dt} = (k_0 + k^{\Delta R}_q[RQ] + k^{\Delta S}_q[SQ])[\Delta Ln^*] \quad (7)$$

Under the conditions employed in our experiments, the relative

(10) Cahn, R. S.; Ingold, C.; Prelog, V. *Angew. Chem., Int. Ed. Engl.* **1966**, *5*, 385–415.

(11) (a) Riehl, J. P.; Richardson, F. S. *Chem. Rev.* **1986**, *86*, 1–16. (b) Richardson, F. S. *J. Less-Common Met.* **1989**, *149*, 161–177.

and absolute concentrations of RQ and SQ may be assumed to remain essentially constant throughout our measurement periods, and eqs 6 and 7 may be integrated to obtain

$$[\Lambda Ln^*]^t = [\Lambda Ln^*]^0 e^{(-k_0 - k_q^{\Delta R}[RQ] - k_q^{\Delta S}[SQ])t} \quad (8)$$

$$[\Delta Ln^*]^t = [\Delta Ln^*]^0 e^{(-k_0 - k_q^{\Delta R}[RQ] - k_q^{\Delta S}[SQ])t} \quad (9)$$

where the superscripts on $[\Lambda Ln^*]^t$ and $[\Delta Ln^*]^t$ denote time after excitation, and it is assumed that $[RQ] = [RQ]^0 = [RQ]^t$ (and similarly for [SQ]). Since the initially prepared Ln* excited-state population is racemic and, therefore, $[\Lambda Ln^*]^0 = [\Delta Ln^*]^0$, the ratio of $[\Lambda Ln^*]^t$ to $[\Delta Ln^*]^t$ is given by

$$\frac{[\Lambda Ln^*]^t}{[\Delta Ln^*]^t} = e^{(k_q^{\Delta R} - k_q^{\Delta R})[RQ]t} e^{(k_q^{\Delta S} - k_q^{\Delta S})[SQ]t} \quad (10)$$

This ratio is related to enantiomeric excess in the Ln* population according to

$$\frac{[\Lambda Ln^*]^t}{[\Delta Ln^*]^t} = \frac{1 + \eta^t_{Ln^*}}{1 - \eta^t_{Ln^*}} \quad (11)$$

where $\eta^t_{Ln^*}$ is defined according to eq 5. Combinings eqs 10 and 11 yields

$$\eta^t_{Ln^*} = \frac{e^{k_{\delta q}^R[RQ]t} - e^{-k_{\delta q}^S[SQ]t}}{e^{k_{\delta q}^R[RQ]t} + e^{-k_{\delta q}^S[SQ]t}} \quad (12)$$

where $k_{\delta q}^R = k_q^{\Lambda R} - k_q^{\Delta R}$ and $k_{\delta q}^S = k_q^{\Delta S} - k_q^{\Lambda S}$. The $k_{\delta q}^R$ and $k_{\delta q}^S$ parameters reflect differential (enantioselective) quenching rates for the RQ and SQ quenching species, respectively.[12] If RQ and SQ were true enantiomers (optical antipodes), then $k_{\delta q}^R$ and $k_{\delta q}^S$ would be equal in magnitude but opposite in sign.

For a sample that contains equimolar concentrations of RQ and SQ diastereomers (i.e., [RQ] = [SQ]), the rate constants for ΛLn^* and ΔLn^* quenching are given by

$$k_q^\Lambda = \tfrac{1}{2}(k_q^{\Lambda R} + k_q^{\Lambda S}) \quad (13)$$

$$k_q^\Delta = \tfrac{1}{2}(k_q^{\Delta R} + k_q^{\Delta S}) \quad (14)$$

The difference between these rate constants may be expressed as

$$k_{\delta q} = k_q^\Delta - k_q^\Lambda = \tfrac{1}{2}(k_{\delta q}^R + k_{\delta q}^S) \quad (15)$$

and eq 12 may be then written as

$$\eta^t_{Ln^*} = (e^{k_{\delta q}[Q]t} - 1)/(e^{k_{\delta q}[Q]t} + 1) \quad (16a)$$

$$= \tanh(k_{\delta q}[Q]t/2) \quad (16b)$$

where [Q] = [RQ] + [SQ] and tanh denotes a hyperbolic tangent function. It will be of further use to define two additional parameters

$$k_q = \tfrac{1}{2}(k_q^\Lambda + k_q^\Delta) \quad (17)$$

$$E_q = \frac{k_q^\Lambda - k_q^\Delta}{k_q^\Lambda + k_q^\Delta} = \frac{-k_{\delta q}}{2k_q} \quad (18)$$

which we shall refer to as the *mean quenching constant* (k_q) and the *enantioselectivity quenching parameter* (E_q). The ratio of k_q^Λ to k_q^Δ is related to k_q, $k_{\delta q}$, and E_q according to

$$\frac{k_q^\Lambda}{k_q^\Delta} = \frac{2k_q - k_{\delta q}}{2k_q + k_{\delta q}} = \frac{1 + E_q}{1 - E_q} \quad (19)$$

Expressions 16, 18, and 19 remain valid if [RQ] ≠ [SQ], but eqs 13–15 must then be reexpressed as follows:

$$k_q^\Lambda = \frac{k_q^{\Lambda R}[RQ] + k_q^{\Lambda S}[SQ]}{[Q]} \quad (20)$$

$$k_q^\Delta = \frac{k_q^{\Delta R}[RQ] + k_q^{\Delta S}[SQ]}{[Q]} \quad (21)$$

$$k_{\delta q} = k_q^\Delta - k_q^\Lambda = \frac{k_{\delta q}^R[RQ] + k_{\delta q}^S[SQ]}{[Q]} \quad (22)$$

Chiroptical Luminescence Measurements. The quantities measured in our chiroptical luminescence experiments are those defined by eqs 1–3. The relationship between emission dissymmetry and excited-state enantiomeric excess is given in eq 4, and this equation may be combined with eq 16b to obtain

$$g_{em}(\lambda',t) = g_{em}^\Lambda(\lambda') \tanh(k_{\delta q}[Q]t/2) \quad (23)$$

where $k_{\delta q}$ is defined by eq 22 *or* by eq 15 (if [RQ] = [SQ]). Expressions for the total luminescence and circularly polarized luminescence intensities are given as follows:[2,3]

$$I(\lambda',t) = \tfrac{1}{2}I(\lambda',0)e^{-(k_0 + k_q[Q])t}[e^{k_{\delta q}[Q]t/2} + e^{-k_{\delta q}[Q]t/2}] \quad (24)$$

$$\Delta I(\lambda',t) = \tfrac{1}{4}g_{em}^\Lambda(\lambda')I(\lambda',0)e^{-(k_0 + k_q[Q])t}[e^{k_{\delta q}[Q]t/2} - e^{-k_{\delta q}[Q]t/2}] \quad (25)$$

where k_0 is the emission decay constant for the Ln* luminophores in the *absence* of quencher species and k_q is the "mean" quenching constant defined by eq 17. The value of k_0 is determined from time-resolved TL measurements on samples in which [Q] = 0, and the k_q and $k_{\delta q}$ parameters are evaluated by fitting time-resolved TL, CPL, and emission dissymmetry data to eqs 23–25. When these data fits are performed, the values of k_0 and [Q] are known for the Ln*–Q system of interest, but the value of $g_{em}^\Lambda(\lambda')$ may not be known. However, this quantity can be treated as an additional fitting parameter in the data analysis, and its magnitude (but not its sign) can be determined.[2] The signs of $k_{\delta q}$ and $g_{em}^\Lambda(\lambda')$ are correlated in the analysis, so ambiguity in the sign of $g_{em}^\Lambda(\lambda')$ leads to ambiguity in the sign of $k_{\delta q}$. Only the sign of $k_{\delta q}g_{em}^\Lambda(\lambda')$ can be determined unambiguously from the empirical data. In the present study, we report values for k_0, k_q, $|k_{\delta q}|$, $|g_{em}^\Lambda(\lambda')|$, and $|E_q|$ (defined by eq 18), and we also report signs for the $k_{\delta q}g_{em}^\Lambda(\lambda')$ products.

Expressions analogous to eqs 23–25 may be developed for *steady-state* excitation/emission detection measurements. The steady-state emission dissymmetry factors are given by

$$\bar{g}_{em}(\lambda') = g_{em}^\Lambda(\lambda')\left[\frac{k_{\delta q}[Q]/2}{k_0 + k_q[Q]}\right] \quad (26)$$

and the steady-state CPL intensities are

$$\overline{\Delta I}(\lambda') = \tfrac{1}{2}\left[\frac{k_{\delta q}[Q]/2}{k_0 + k_q[Q]}\right] g_{em}^\Lambda(\lambda')\bar{I}(\lambda') \quad (27)$$

where $\bar{I}(\lambda')$ denotes the steady-state TL intensity. Under steady-state conditions, enantioselective quenching produces an enantiomeric excess in the Ln* population given by

$$\bar{\eta}_{Ln^*} = \frac{k_{\delta q}[Q]/2}{k_0 + k_q[Q]} \quad (28)$$

Spectroscopic Properties of Complexes

$Eu(dpa)_3^{3-}$. Luminescence spectra of $Eu(dpa)_3^{3-}$ in neutral aqueous solution may be assigned to transitions originating from the nondegenerate $^5D_0$ multiplet of the $4f^6$ (Eu^{3+}) electronic configuration. This multiplet is located at 17240 cm^{-1} above the $^7F_0$ *ground* multiplet, and a $^5D_0$ luminescence spectrum exhibits six distinct transition regions assigned to $^7F_J \leftarrow {}^5D_0$ (J = 1, 2, 3, 4, 5, 6) multiplet-to-multiplet transition manifolds (the $^7F_0 \leftarrow {}^5D_0$ transition is forbidden in D_3 symmetry). The most intense luminescence is observed in the $^7F_2 \leftarrow {}^5D_0$ and $^7F_4 \leftarrow {}^5D_0$ transition regions, but the strongest chiroptical activity (i.e., the largest emission dissymmetry) is observed in the $^7F_1 \leftarrow {}^5D_0$ luminescence.

(12) The $k_{\delta q}$ parameters defined here are identical to the k_d parameter of refs 2 and 3.

In this study, we focus primarily on chiroptical measurements in the $^7F_1 \leftarrow {}^5D_0$ transition region (586–597 nm), with special emphasis on the crystal-field component at 594.8 nm. In our experiments, excitation was at 465.8 nm, which coincides with a $^7F_0 \rightarrow {}^5D_2$ absorption line of $Eu(dpa)_3^{3-}$. The $^5D_2$ excited-state population rapidly decays to the $^5D_0$ emitting level (the $^5D_2$ and $^5D_0$ multiplets are only separated by ca. 4210 cm^{-1}), and for $Eu(dpa)_3^{3-}$, and lifetime of the $^5D_0$ level is 1.61 ms in H_2O and 3.20 ms in D_2O solutions.

$Tb(dpa)_3^{3-}$. Luminescence spectra of $Tb(dpa)_3^{3-}$ complexes in neutral aqueous solution may be assigned to transitions originating from crystal-field levels split out of the $^5D_4$ multiplet of the $4f^8$ (Tb^{3+}) electronic configuration. The baricenter of this multiplet is located approximately 20 370 cm^{-1} above the baricenter of the $^7F_6$ *ground* multiplet of $4f^8$ (Tb^{3+}), and a $^5D_4$ luminescence spectrum exhibits seven distinct transition regions that may be assigned to $^7F_J \leftarrow {}^5D_4$ ($J = 0, 1, 2, 3, 4, 5, 6$) multiplet-to-multiplet transition manifolds. The most intense emission is observed in the $^7F_5 \leftarrow {}^5D_4$ transition region, and this region also exhibits relatively strong chiroptical properties (CPL and emission dissymmetry). The $^7F_5 \leftarrow {}^5D_4$ luminescence spans the 535–555-nm wavelength range, and all of the chiroptical luminescence measurements reported for $Tb(dpa)_3^{3-}$ in this study, were obtained within the $^7F_5 \leftarrow {}^5D_4$ transition region. Excitation was at 488 nm, which falls within the $^7F_6 \rightarrow {}^5D_4$ absorption region of $Tb(dpa)_3^{3-}$. The lifetime of the $^5D_4$ emitting levels is 2.13 ms for $Tb(dpa)_3^{3-}$ in H_2O and 2.21 ms in D_2O.

$Co(NH_3)_4$(nucleotide) Complexes. The spectroscopic properties of the $Co(NH_3)_4$(ntp) and $Co(NH_3)_4$(ndp) complexes are of interest here *only* insofar as they are related to the quenching of $Eu(dpa)_3^{3-}$ and $Tb(dpa)_3^{3-}$ luminescence. The quenching mechanism involves resonance energy transfer from Ln* donor states to Q acceptor states, and this energy transfer presumably (but not necessarily) occurs within Ln*–Q collisional complexes.[2,4] The donor state of the Eu* complexes is $^5D_0$ ($4f^6$), and the donor state of the Tb* complexes is $^5D_4$ ($4f^8$). These states are located at approximately 17 240 and 20 370 cm^{-1}, respectively, above ground. Among the Co(III) complexes employed as quenchers in this study, the only suitable acceptor levels for Ln*-to-Q electronic energy transfer are those derived from the $3d^6$ (Co^{3+}) electronic configuration. Ligand-localized states and ligand-to-metal charge-transfer states are too high in energy to meet the required resonance conditions.

The lowest-energy *spin-allowed* d–d absorption band observed for the $Co(NH_3)_4$(nucleotide) complexes spans the 470–600-nm wavelength range, with a λ_{max} that varies between 515 and 560 nm (depending on the nucleotide ligand). This band exhibits an ϵ_{max} of ca. 70 M^{-1} cm^{-1}, and it may be assigned to d–d transitions of $^1A_{1g} \rightarrow {}^1T_{1g}$ octahedral (O_h) parentage. This absorption band has good spectral overlap with three Tb* emission manifolds ($^7F_6 \leftarrow {}^5D_4$, $^7F_5 \leftarrow {}^5D_4$, and $^7F_4 \leftarrow {}^5D_4$), and one may assume that the $^1T_{1g}$ state of Co(III) provides acceptor levels for Tb*-to-Co energy transfer. On the other hand, only the long-wavelength tail of the $^1A_{1g} \rightarrow {}^1T_{1g}$ absorption band has any significant overlap with a Eu* emission ($^7F_1 \leftarrow {}^5D_0$), and it seems unlikely that the $^1T_{1g}$ state can play an effective acceptor role in Eu*-to-Co energy transfer. Cobalt(III) complexes are known to have *spin-forbidden* d–d transitions that are lower in energy than the $^1A_{1g} \rightarrow {}^1T_{1g}$ transition,[13] and the weak absorption bands associated with these transitions overlap several Eu* $^7F_J \leftarrow {}^5D_0$ emission manifolds *and* several Tb* $^7F_J \leftarrow {}^5D_4$ emission manifolds. It is likely that the excited states in these spin-forbidden d–d transitions (of *nominal* $^1A_{1g} \rightarrow {}^3T_{2g}$ and $^1A_{1g} \rightarrow {}^3T_{1g}$ octahedral parentage) play a crucial role as acceptor levels in Eu*-to-Co energy transfer, and it is possible that they are also involved in the Tb*-to-Co energy-transfer mechanism.

Experimental Section

Preparation of Complexes. $Eu(dpa)_3^{3-}$ and $Tb(dpa)_3^{3-}$. Stock solutions of $Eu(dpa)_3^{3-}$ and $Tb(dpa)_3^{3-}$ were prepared by reaction of the appropriate lanthanide carbonate, $Eu_2(CO_2)_3$ or $Tb_2(CO_2)_3$, with 6 equiv of dipicolinic acid in H_2O, followed by neutralization of the solution with Na_2CO_3. The solutions were diluted with a pH 6 phosphate buffer[14] to bring the lanthanide concentration to 20 mM. Solutions in D_2O were prepared by evaporating the above solutions under high vacuum and dissolving the resulting solid in D_2O (Aldrich, 99.8 atom % D).

Nucleotide Complexes. The β,γ-bidentate complexes of $Co(NH_3)_4$(ntp) and the α,β-bidentate complexes of $Co(NH_3)_4$(ndp) were prepared by essentially the same method as described by Cleland and co-workers[8a] in their synthesis of $Co(NH_3)_4$(atp). All Co–nucleotides were purified on columns of AG 50W-X2 Dowex (100–200 mesh, H^+ form) in a cold cabinet (4 °C) except for guanosine, which was prepared at room temperature. Concentrations of the Co–nucleotides were determined spectrophotometrically using the following molar extinction coefficients: ϵ_a(257 nm, pH 2) = 15 000 M^{-1} cm^{-1}; ϵ_c(280 nm, pH 2) = 12 800 M^{-1} cm^{-1}; ϵ_g (256 nm, pH 2) = 12 400 M^{-1} cm^{-1}; ϵ_i(248 nm, pH 3) = 12 200 M^{-1} cm^{-1}; ϵ_t(267 nm, pH 3) = 10 200 M^{-1} cm^{-1}; ϵ_u(262 nm, pH 3) = 10 000 M^{-1} cm^{-1}. All samples were treated with Chelex 100 to remove divalent metals. Some samples were prepared in 99+ atom % D_2O by repeated rotatory evaporation. The purity and quality of all Co–nucleotides were verified by ^{31}P NMR at 300 MHz. Chemical shifts (relative to external 100 mM H_3PO_4) for $Co(NH_3)_4$(ntp) were P_γ = 4.0 ppm, P_β = −10.4 ppm, and P_α = −10.9 ppm; and for the $Co(NH_3)_4$(ndp), P_β = 4.3 ppm and P_α = 1.1 ppm. The resonances for P_β in the $Co(NH_3)_4$(ntp) complexes and P_α in the $Co(NH_3)_4$(ndp) complexes are split due to the nonequivalence of the phosphates in the two diastereomeric forms associated with the absolute configuration about these phosphates, and integration of the two resonances showed that the mixtures of diastereomers are racemic with respect to the configurational chirality about these phosphates. Samples were stored at −20 °C, and used within 1 month of synthesis.

The final concentrations of solutions used for spectral runs were 50 or 100 μM for the di- or triphosphates, respectively; 10 mM for the $Ln(dpa)_3^{3-}$ complexes; and 100 μM for PO_4^{3-} from the phosphate buffer.

Instrumentation and Measurement Techniques. The instrumental methods used in this study have been described previously.[2,3] Emission and CPL spectra were recorded on an instrument constructed at the University of Virginia. The sample was held in a water-jacketed 1-cm fluorescence cuvette and the temperature controlled to ±0.1 °C with a circulating bath. For excitation, we used either the 465.8-nm line (for excitation of the $^7F_0 \rightarrow {}^5D_2$ transition of Eu^{3+}) or the 488-nm line (for excitation of the $^7F_6 \rightarrow {}^5D_4$ transition of Tb^{3+}) of an argon ion laser. For the time-resolved studies, the excitation beam was mechanically chopped at a frequency of 51 Hz. The time-resolved measurements reported in this study involved data collection over a period of hours; sample stability was checked by measuring decay characteristics before and after each spectral run.

Data Manipulation and Deconvolution. Of numerical interest in this study is the determination of k_0, k_q, k_{bq}, and $g_{em}^{\Delta}(\lambda')$ for each $Co(NH_3)_4$(nucleotide)–$Ln(dpa)_3^{3-}$ combination. During the time-resolved measurements, we simultaneously acquire $I(\lambda',t)$ and $\Delta I(\lambda',t)$ data, from which is calculated $g_{em}(\lambda',t)$ data (see eq 3). The k_0 and k_q parameters are determined by fitting $I(\lambda',t)$ data to the *single-exponential equation*

$$I(\lambda',t) = I(\lambda',0)e^{-(k_0+k_q[Q])t} + dc \qquad (29)$$

The final term in this equation is a correction for dark counts (dc) in the total luminescence data. (The unquenched total luminescence lifetime k_0 is determined with no quencher present.) The previously derived equation for the decay of $I(\lambda',t)$ (eq 24) is a *double-exponential* equation, with rate constants of $k_0 + (k_q \mp k_{bq}/2)[Q]$. For cases where k_{bq} is small compared to k_q, fitting of the $I(\lambda',t)$ data to eq 29 will lead to good values of the mean quenching constant, k_q. Values of k_{bq} and $g_{em}^{\Delta}(\lambda')$ are determined by fitting $g_{em}(\lambda',t)$ data to the equation

$$g_{em}(\lambda',t) = g_{em}^{\Delta}(\lambda') \tanh (k_{bq}[Q]t/2)\frac{I(\lambda',t) - dc}{I(\lambda',t)} \qquad (30)$$

This is eq 23, with the final term being a correction for dark counts in the $I(\lambda',t)$ data (the denominator in the $g_{em}(\lambda',t)$ calculation).

The plots of $g_{em}(\lambda',t)$ vs t will have the form of a tanh function, with increasing values of $g_{em}(\lambda',t)$ up to some asymptotic limit, which represents the limiting $|g_{em}^{\Delta}(\lambda')|$ value for fully resolved $Eu(dpa)_3^{3-}$ or $Tb(dpa)_3^{3-}$ complex. Fitting the latter portion of the $g_{em}(\lambda',t)$ plot will lead to well-determined values of $|g_{em}^{\Delta}(\lambda')|$. This can be somewhat difficult, since at long times in the emission decay there is not much emission, and dark counts and noise in the data become significant.

(13) Wilson, R. B.; Solomon, E. I. *J. Am. Chem. Soc.* **1980**, *102*, 4085–4095.

(14) Perrin, D. D.; Dempsey, B. *Buffers for pH and Metal Ion Control*; Wiley: New York, 1974.

We use Marquardt-based, nonlinear least-squares algorithms for fitting of the experimental time-resolved data to the above-derived equations.[15] The dark count term in each can be estimated from instrumental characteristics or used as an additional fitting parameter.

Results

General Results. In this section and hereafter we will continue to use an abbreviated notation for the two lanthanide complexes, Eu for $Eu(dpa)_3^{3-}$ and Tb for $Tb(dpa)_3^{3-}$, and we will also use the generic notations Ln and Q for the lanthanide complexes and quencher species, respectively. At various times, we will also use the contracted notation CoNTP and CoNDP for $Co(NH_3)_4$(ntp) and $Co(NH_3)_4$(ndp) complexes, respectively.

All of the results reported here were obtained on samples that contained approximately *equimolar* concentrations of the *R* and *S* diastereomers of the $Co(NH_3)_4$(nucleotide) complexes. Recall from our earlier discussion that the *R* and *S* labels identify the absolute configuration about the asymmetric phosphorus atom of the six-membered Co–nucleotide bidentate chelate ring, and they correspond to Cleland's Λ and Δ labels, respectively.[8c,9] Both the *R* and *S* diastereomer concentrations contain subpopulations of structural isomers that may differ with respect to chelate ring conformation *and* variations in the spatial orientation and conformational properties of the nucleoside base and sugar moieties. These subpopulations of structural isomers are not considered *explicitly* in our kinetic model for quenching (see Theory and Measurement Methodology section), and our quenching measurements yield values for the *differential and mean* quenching constants, $k_{\delta q}$ and k_q, defined by eqs 15 and 17, respectively. Furthermore, recall from earlier discussion that only the magnitude, but *not* the sign, of $k_{\delta q}$ can be determined from our measurements, although both the magnitude *and* sign of $k_{\delta q}g_{em}^{\Lambda}(\lambda')$ can be determined (see discussion following eqs 23–25). The principal results reported in the following sections are time-resolved TL, CPL, and emission dissymmetry data, values for the k_0, k_q, and $|k_{\delta q}|$ rate parameters (see eqs 23–25), values for $|E_q|$ and $|g_{em}^{\Lambda}(\lambda')|$ (see eqs 18 and 23), and signs of $k_{\delta q}g_{em}^{\Lambda}(\lambda')$ products.

Measurements were carried out on neutral aqueous (H_2O or D_2O) solution samples (at 4 and 20 °C) that contained 100 μM phosphate buffer, a luminophore concentration of 10 mM, and a quencher concentration of 50 μM for the CoNDP complexes and 100 μM for the CoNTP complexes. The results obtained for H_2O vs D_2O solution samples were essentially identical, and results obtained at sample temperatures of 4 and 20 °C were also essentially identical, although some evidence for quencher decomposition was noted for the 20 °C experiments. Data acquisition conditions were optimal for the D_2O solution samples at 4 °C, and most of the data we show in this paper are for those samples. The *unquenched* lifetimes of $Eu(dpa)_3^{3-}$ and $Tb(dpa)_3^{3-}$ are longer in D_2O vs H_2O solutions (3.20 vs 1.61 ms for Eu*, and 2.21 vs 2.13 for Tb*, at 4 °C), and the longer lifetimes permit longer periods over which quenching processes may be observed. Satisfactory data sets were obtained for both H_2O and D_2O solutions at 4 and 20 °C, but the data obtained for D_2O solutions at 4 °C were superior with respect to quality and quantity. We note again, however, that the k_q and $k_{\delta q}$ rate parameters derived from analyses of the various data sets do not show any significant solvent or temperature dependence.

Spectra. The spectral dispersion characteristics of the total luminescence measured for the $Eu(dpa)_3^{3-}$ and $Tb(dpa)_3^{3-}$ complexes are not altered by the addition of quencher complexes to a solution sample. Furthermore, the circularly polarized luminescence generated by enantioselective quenching exhibits spectral dispersion characteristics identical to those observed in CPL generated by circularly polarized excitation of the Eu and Tb complexes in the *absence* of any chiral reagents. These results indicate that the TL and CPL observed in our experiments derive entirely from Eu* and Tb* complexes that are free of any perturbations by the cobalt complexes. The latter complexes act only as excited-state quenchers that deplete the population of Eu* or Tb* luminophores and thereby reduce the mean luminescence lifetime (and intensity).

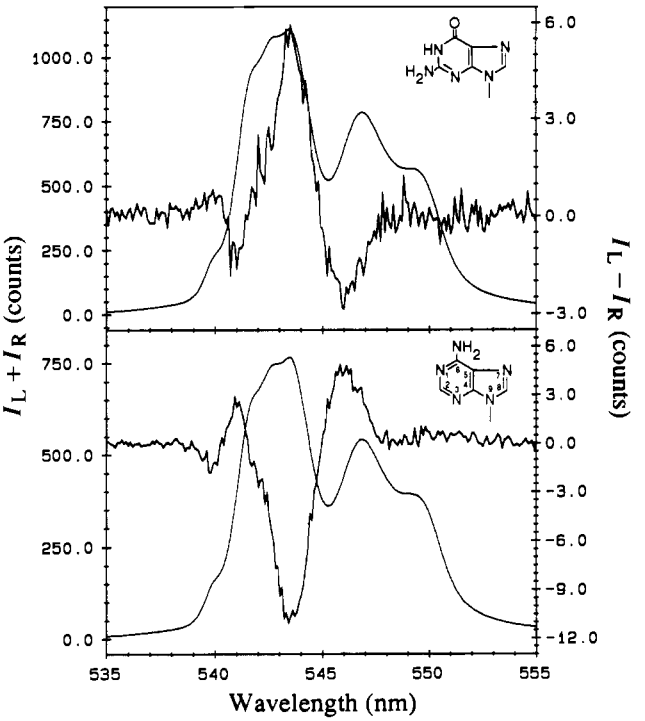

Figure 2. Time-integrated CPL and TL spectra for $Tb(dpa)_3^{3-}$–$Co(ND_3)_4$(nucleotide) systems in D_2O at 4 °C. The top frame shows spectra for 10 mM $Tb(dpa)_3^{3-}$ and 100 μM $Co(ND_3)_4$(gtp), and the bottom frame shows spectra for 10 mM $Tb(dpa)_3^{3-}$ and 100 μM $Co(ND_3)_4$(atp). The noisy trace in each represents the CPL ($I_L - I_R$), and the smooth trace in each represents the TL ($I_L + I_R$). These samples were excited at 488 nm.

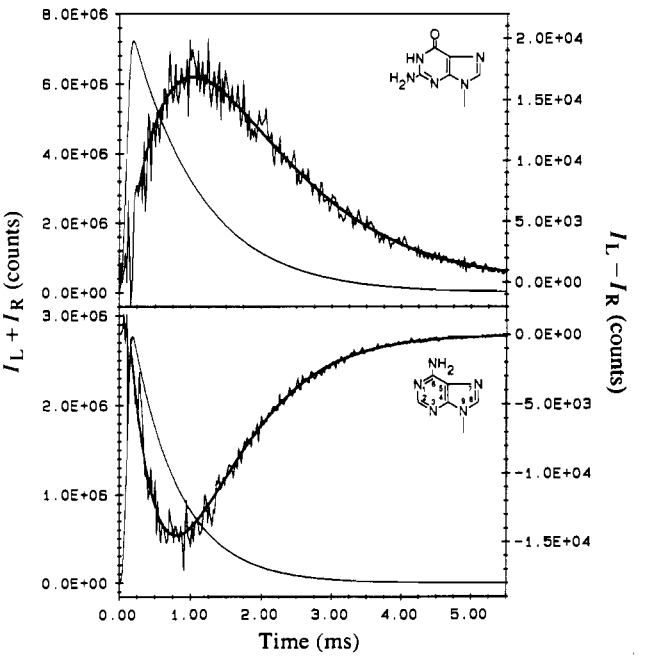

Figure 3. Time-resolved CPL and TL scans for the systems shown in Figure 2. The emission wavelength for these scans was 543.7 nm, and the excitation wavelength was 488 nm.

Examples of TL and CPL spectra are shown in Figure 2 for the $^7F_5 \leftarrow {}^5D_4$ transition region of Tb*. These spectra were obtained for D_2O solutions in which [Tb] = 10 mM, [Q] = 100 μM, and the quencher was either $Co(ND_3)_4$(atp) (bottom spectra) or $Co(ND_3)_4$(gtp) (top spectra). Note the mirror-image relationship between the *signs* of the CPL ($\Delta I = I_L - I_R$) observed for the Tb*–CoATP vs Tb*–CoGTP systems and also note that

(15) Press, W. H.; Flannery, B. P.; Teukolsky, S. A.; Vetterling, W. T. *Numerical Recipes in Pascal*; Cambridge University Press: Cambridge, UK, 1989.

Table I. Parameter Values Determined from Analyses of CPL and TL Data for D_2O Experiments[a]

Ln*	Co–nucleotide complex[b]	k_0, s^{-1}	$10^{-6}k_q$, M^{-1} s^{-1}	$10^{-6}\lvert k_{\delta q}\rvert$, M^{-1} s^{-1}	$\lvert g_{em}^{\Lambda}(\lambda')\rvert$[c]	sign of $k_{\delta q}g_{em}^{\Lambda}(\lambda')$	$10^2\lvert E_q\rvert$	$(1+\lvert E_q\rvert)/(1-\lvert E_q\rvert)$[d]
$Tb(dpa)_3^{3-}$	atp	452.5	10.7	2.9	0.28	−	13.7	1.32
	adp		14.4	0.086	0.28	+	0.3	1.01
	gtp		5.86	0.80	0.28	+	6.8	1.15
	gdp		10.7	1.39	0.28	+	6.5	1.14
	itp		4.28	0.46	0.28	+	4.6	1.10
	idp		8.36	0.60	0.28	+	3.6	1.07
	ctp		6.10	0.080	0.28	−	0.7	1.02
	utp		5.35	0.27	0.28	−	2.6	1.05
	ttp		5.45	0.36	0.28	−	3.3	1.07
$Eu(dpa)_3^{3-}$	atp	312.5	10.4	2.7	0.24	−	13.0	1.30
	adp		16.9	0.12	0.24	+	0.4	1.01
	gtp		2.52	0.36	0.24	+	7.1	1.15
	gdp		4.51	0.80	0.24	+	8.9	1.20
	itp		2.22	0.11	0.24	+	2.5	1.05
	idp		4.55	0.28	0.24	+	3.1	1.06
	ctp		2.90	0.041	0.24	−	0.7	1.02
	utp		2.59	0.12	0.24	−	2.3	1.05
	ttp		2.54	0.30	0.24	−	5.9	1.13

[a] Parameter definitions are given in the Theory and Measurement Methodology section of the text. Data measured for D_2O solutions at 4 °C. Concentrations of the $Ln(dpa)_3^{3-}$ complexes were 10 mM; for the ntp quenchers, 100 μM; and for the ndp quenchers, 50 μM. [b] Each nucleotide complex is of stoichiometry $Co(NH_3)_4$(nucleotide) and is identified by the abbreviation for the nucleotide. [c] For Tb*, $\lambda' = 543.7$ nm. For Eu*, $\lambda' = 594.8$ nm. [d] This quantity is defined according to eq 19 in the text, and it corresponds to *either* $k_q^{\Lambda}/k_q^{\Delta}$ (if $k_q^{\Lambda} \geq k_q^{\Delta}$) *or* $k_q^{\Delta}/k_q^{\Lambda}$ (if $k_q^{\Delta} \geq k_q^{\Lambda}$).

the *magnitude* of the CPL/TL intensity ratio ($\Delta I/I$) at any given wavelength is greater for Tb*–CoATP than for Tb*–CoGTP. The mirror-image sign relationship reflects opposite enantiomeric preferences in Tb*–CoATP vs Tb*–CoGTP quenching processes, and differences in the magnitude of CPL/TL intensity ratios reflect differences between the enantioselective and total quenching efficiencies in Tb*–CoATP vs Tb*–CoGTP. Time-resolved TL and CPL (monitored at $\lambda' = 543.7$ nm) are shown in Figure 3 for Tb*–CoATP (bottom panel) and Tb*–CoGTP (top panel) systems in D_2O. Note that the Tb*–CoATP system exhibits faster emission decay kinetics (more efficient quenching). The lag of the CPL maximum intensity as compared to the TL maximum intensity is reflective of the dynamic enantioselective quenching process which is responsible for the observation of CPL from these systems. Plots of g_{em} vs time calculated from these data (and data from the other systems) are not shown here, but do demonstrate that at times close to that of the excitation pulse there is no detectable enantiomeric excess in the *excited-state* population (and hence the *ground-state* population) of $Ln(dpa)_3^{3-}$ luminophores ($g_{em} = 0$ at $t = 0$). The g_{em} vs t plots have the same general appearance as is shown in Figures 5, 7, and 8 of ref 2.

Luminescence Quenching Parameters. Results obtained from analyses of CPL and TL measurements on D_2O solution samples at 4 °C are summarized in Table I. As was discussed earlier in the paper, the magnitudes but not the signs of the $k_{\delta q}$, $g_{em}^{\Lambda}(\lambda')$, and E_q parameters can be determined from our measurements, whereas both the magnitude *and* sign of the product quantity $k_{\delta q}g_{em}^{\Lambda}(\lambda')$ can be determined. Opposite signs for this quantity correspond to opposite preferences in ΛLn*–Q vs ΔLn*–Q quenching interactions. For chiral quencher molecules that exist in just two, well-defined, enantiomeric structural forms (with either a left-handed or a right-handed absolute configuration), opposite enantiomers of the quencher molecule must *necessarily* produce $k_{\delta q}g_{em}^{\Lambda}(\lambda')$ values that are equal in magnitude but opposite in sign.[2-4] For a series of quencher molecules that are chemically distinct but are similar with respect to their electronic and stereochemical structure (*including* chirality), one would predict $k_{\delta q}g_{em}^{\Lambda}(\lambda')$ values of *like* sign with similar (but not identical) magnitudes.[2,3] The CoNDP and CoNTP quencher complexes examined in this study have similar electronic and stereochemical structures in their $Co(NH_3)_4$(phosphate) moiety, and at least two parts of their structural chirality derive from common sources: the asymmetric phosphorus atom in the Co–phosphate chelate ring and the asymmetric carbon atoms in the ribosyl moiety. Given these structural similarities, one might expect that all of the $k_{\delta q}g_{em}^{\Lambda}(\lambda')$ quantities listed in Table I would have the same sign. However, in both the Eu* and Tb* quenching experiments, the adp, gtp, gdp, itp, and idp complexes of $Co(NH_3)_4$(nucleotide) produced $k_{\delta q}g_{em}^{\Lambda}(\lambda')$ values of *positive* sign, whereas the atp, ctp, utp, and ttp complexes gave $k_{\delta q}g_{em}^{\Lambda}(\lambda')$ values of *negative* sign. These results imply that the purine or pyrimidine base moiety of the nucleotide ligand has a decisive influence on the chiral discrimination processes responsible for enantioselective quenching.

The absolute sign of the E_q (enantioselectivity) quenching parameter cannot be determined from our measurements, but the *relative* signs of E_q values for different systems can be correlated with the relative signs of the $k_{\delta q}g_{em}^{\Lambda}(\lambda')$ quantities. The magnitude of E_q is given by $\lvert k_{\delta q}/2k_q\rvert$ (see eq 18), and values of $\lvert E_q\rvert$ may range from 0 (*no* enantioselectivity in the quenching) to 1 (*maximal* enantioselectivity in the quenching). According to eq 19, the ratio of $1+\lvert E_q\rvert$ to $1-\lvert E_q\rvert$ is equal to *either* $k_q^{\Lambda}/k_q^{\Delta}$ (if $k_q^{\Lambda} \geq k_q^{\Delta}$) *or* $k_q^{\Delta}/k_q^{\Lambda}$ (if $k_q^{\Lambda} \leq k_q^{\Delta}$). (Note that the *sign* of either $k_{\delta q}$ or E_q must be known to determine the larger of the k_q^{Λ} and k_q^{Δ} parameters). The results given in Table I show significant variations among the $\lvert E_q\rvert$ values determined for the different CoNDP and CoNTP quencher complexes, and these variations are similar in the Eu* and Tb* data sets. The variations observed within the Eu* and Tb* data sets give further evidence that the base moiety of the nucleotide ligand plays a major role in ΛLn*–Q vs ΔLn*–Q discriminatory interactions, and the similarities between the Eu* and Tb* data sets indicate that these chiral discriminatory interactions are relatively insensitive to the *electronic* properties of the respective lanthanide luminophores. The $Eu(dpa)_3^{3-}$ and $Tb(dpa)_3^{3-}$ complexes are expected to have essentially identical stereochemical structures, but Eu^{3+} ($4f^6$) and Tb^{3+} ($4f^8$) have very different $4f^N$ electronic-state structures and 4f–4f optical emission properties.

The *mean* quenching constant k_q does not contain any information about chiral discriminatory interactions, but it does provide a useful measure of the relative quenching abilities of the various CoNDP and CoNTP complexes. From the k_q data given in Table I, we note first that the CoNDP complexes are stronger quenchers than their CoNTP counterparts (for any given *purine* nucleoside, N ≡ A, G, or I). This differentiation is most likely attributable to the relative net charges (ze) that can be formally assigned to the CoNDP ($z = 0$) vs CoNTP ($z = -1$) complexes. The neutral CoNDP complexes are expected to interact more strongly with the $Ln(dpa)_3^{3-}$ luminophores than will the negatively charged CoNTP complexes, and one may expect that the Ln*–CoNDP *encounter* complexes formed in solution will be more stable (and longer-lived) than the Ln*–CoNTP *encounter* complexes. If one further assumes that these encounter complexes are necessary precursors to the main quenching event (Ln*-to-Q electronic energy transfer), then the relative quenching abilities of the

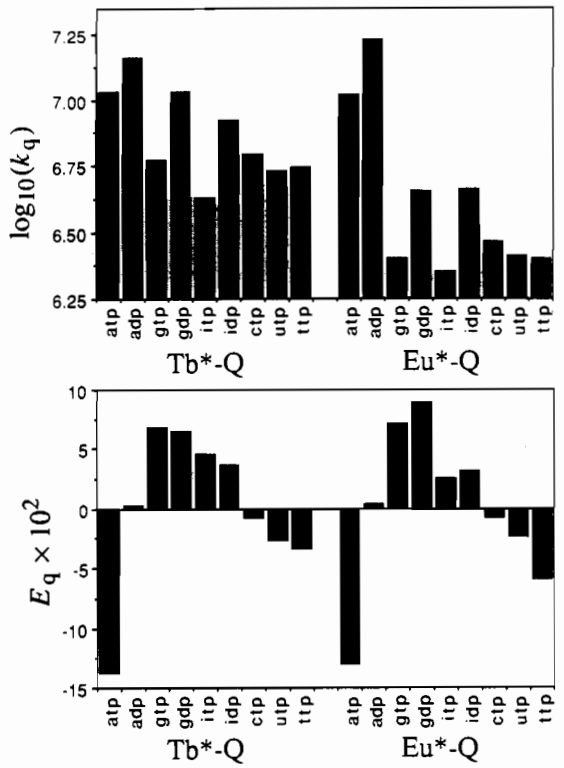

Figure 4. Bar-graph plots of log k_q and E_q data from Table I. The *relative* signs of the E_q parameters for the different systems are taken as the signs of the $k_{\delta q}g^{\Delta}_{em}(\lambda')$ products for each, which are directly determinable from the experimental data (see Measurement and Methodology section).

CoNDP vs CoNTP complexes can be rationalized (at least in part) by their relative charge properties.

The k_q data in Table I also show clear differentiation between Eu*–Q and Tb*–Q quenching rates. With only two exceptions, the k_q(Tb*–Q) rate constants are larger than the k_q(Eu*–Q) rate constants by a factor of 1.8 or more. The two exceptions are for Q ≡ CoADP and Q ≡ CoATP, where k_q(Tb*–Q) and k_q(Eu*–Q) have comparable values. The exceptional quenching behavior of CoADP and CoATP is not confined to the k_q(Tb*–Q) vs k_q(Eu*–Q) comparison. We note also that (1) these complexes give the *largest* k_q(Tb*–Q) and k_q(Eu*–Q) values measured in our study, (2) the CoATP complex gives the *largest* values for E_q(Tb*–Q) and E_q(Eu*–Q), and (3) the CoADP complex gives the *smallest* values for E_q(Tb*–Q) and E_q(Eu*–Q). These exceptional quenching properties of CoADP and CoATP imply structural properties that are unique among the Co(NH$_3$)$_4$(nucleotide) complexes examined in this study.

The k_q and E_q data of Table I are presented in a bar-graph format in Figure 4. Note that the k_q data are graphed as log k_q, and the relative signs of the E_q parameter values have been chosen to conform to the relative signs of the $k_{\delta q}g^{\Delta}_{em}(\lambda')$ quantities. The main features and trends both *within* and *between* the Tb*–Q and Eu*–Q data sets are easily discernible in the bar graphs of Figure 4, and several of these features have already been identified and discussed earlier in this section. Within the context of the present study, the E_q parameter is of paramount interest, and the salient features of the E_q graphs in Figure 4 may be summarized as follows: (1) the opposite sign of E_q for the adp, gtp, gdp, itp, and idp complexes vs the atp, ctp, utp, and ttp complexes; (2) the generally similar $|E_q|$ values for Tb*–Q vs Eu*–Q quenching; (3) the large $|E_q|$ values for Tb*–CoATP and Eu*–CoATP compared to the very small values of $|E_q|$ for Tb*–CoADP and Eu*–CoADP; and (4) the similarities between CoGTP and CoGDP, *and* between CoITP and CoIDP, as enantioselective quenchers (in contrast to the dissimilarities between CoATP and CoADP). We also note that the *pyrimidine* nucleotide complexes (CoCTP, CoUTP, and CoTTP) have E_q values of the same sign as that for CoATP, but opposite to that for CoGTP and CoITP.

Discussion

The main impetus for this work was our interest in chiral discriminatory interactions between metal complexes in solution and the detection of these interactions via enantioselective luminescence quenching measurements. In previous work,[1-4] we showed that time-resolved chiroptical luminescence spectroscopy provides a sensitive means for monitoring enantioselective quenching dynamics and for measuring the rate parameters associated with the quenching processes. Enantioselective quenching kinetics have now been studied for a variety of systems in which the luminophores are either Eu(dpa)$_3^{3-}$ or Tb(dpa)$_3^{3-}$ complexes in aqueous solution, and the quenchers are resolved (or partially resolved) enantiomers of chiral Co(III), Rh(III), or Ru(II) complexes.[1-4,16,17] A variety of structural shapes, sizes, symmetries, and ligand types are represented among the quencher complexes that have been studied, and the enantioselective quenching kinetics exhibit sensitivity to these structural variations as well as the electronic-state structure of the transition metal. Furthermore, a mechanistic model has been developed for relating the enantioselective quenching parameters to specific aspects of luminophore and quencher structure (stereochemical *and* electronic) and to chiral discriminatory luminophore–quencher (Ln*–Q) interactions.[4] In this model, chiral discriminatory contributions to enantioselective quenching are ascribed to one or more of the following: (a) enantiodifferential interactions in the formation and dissociation of Ln*–Q (transient) encounter complexes in solution, (b) differential geometries and stereochemical preferences in Ln*–Q diastereomeric structures (as dictated by stereoselective contact interactions in the encounter complexes), and (c) chiral discrimination in the interactions that *directly* govern Ln*-to-Q electronic energy-transfer processes. This model presumes that for lanthanide luminophores all quenching occurs via Ln*-to-Q electronic energy-transfer processes *within* Ln*–Q encounter complexes, but it makes no assumptions regarding the detailed interaction mechanism for energy transfer (except that it be short range).

For all of the Ln*–Q systems examined to date, the observed quenching rates are at least 2 orders of magnitude smaller than those expected for diffusion-limited kinetics, no evidence is found for long-lived (static) Ln*–Q or Ln–Q association complexes, and the quenching rate constants may be satisfactorily represented as[4]

$$k_q = K_a k_e \tag{31}$$

where k_e is the rate constant for Ln*-to-Q electronic energy transfer and K_a is a quasi-equilibrium constant associated with the formation and dissociation of Ln*–Q species that are the precursors to energy transfer. This expression may be applied to both the ΛLn* and ΔLn* enantiomers of the luminophore excited-state population to obtain

$$k_q = \tfrac{1}{2}(k_q^{\Lambda} + k_q^{\Delta}) = \tfrac{1}{2}(K_a^{\Lambda}k_e^{\Lambda} + K_a^{\Delta}k_e^{\Delta}) \tag{32}$$

$$k_{\delta q} = k_q^{\Lambda} - k_q^{\Delta} = K_a^{\Lambda}k_e^{\Lambda} - K_a^{\Delta}k_e^{\Delta} \tag{33}$$

$$E_q = \frac{k_q^{\Lambda} - k_q^{\Delta}}{k_q^{\Lambda} + k_q^{\Delta}} = \frac{K_a^{\Lambda}k_e^{\Lambda} - K_a^{\Delta}k_e^{\Delta}}{K_a^{\Lambda}k_e^{\Lambda} + K_a^{\Delta}k_e^{\Delta}} \tag{34}$$

$$\frac{k_q^{\Lambda}}{k_q^{\Delta}} = \frac{K_a^{\Delta}k_e^{\Lambda}}{K_a^{\Delta}k_e^{\Delta}} \tag{35}$$

These expressions, when elaborated with the aid of specific models for K_a^{Λ} vs K_a^{Δ} and k_e^{Λ} vs k_e^{Δ} differentiation, have proved useful in previous analyses of enantioselective quenching kinetics.

The experiments performed in the present work are similar to those performed in our previous studies of enantioselective quenching, the chiral luminophore systems are identical to those used previously, and the *mean* quenching rate constants (k_q)

(16) Metcalf, D. H.; Bolender, J. P.; Richardson, F. S., manuscript in preparation.
(17) Metcalf, D. H.; Stewart, J. McD.; Richardson, F. S., unpublished results.

measured in the present study are smaller but of the same order of magnitude as those measured previously for Co(III) quenchers of $Eu(dpa)_3^{3-}$ and $Tb(dpa)_3^{3-}$ luminescence. The smaller k_q values measured in the present study for CoNDP and CoNTP quencher complexes undoubtedly reflect the neutral ($z = 0$) or negatively charged ($z = -1$) nature of these complexes vs the positively charged ($z = +3$) nature of the Co(III) quencher complexes used in the previous studies.[2,4,16] With negatively charged ($z = -3$) luminophores, one may expect that the K_a parameter of eq 31 will increase with increasing positive charge on the quencher species.

In our previous studies of Eu*–Co and Tb*–Co systems, we generally found that the k_q rate constants for Tb*–Co quenching were larger than those for Eu*–Co quenching (for any given Co(III) quencher complex), and this was attributed to the more favorable resonance conditions for Tb*-to-Co vs Eu*-to-Co electronic energy-transfer processes.[2] The donor and acceptor states in Tb*–Co systems match up better (energetically) than do the donor and acceptor states in Eu*–Co systems, and one may expect that the k_e rate parameter of eq 31 will be larger for Tb*–Co systems than for Eu*–Co systems. However, for any given Co(III) quencher complex, the K_a parameter of eq 31 is expected to be the same for Tb*–Co and Eu*–Co systems since the $Tb(dpa)_3^{3-}$ and $Eu(dpa)_3^{3-}$ complexes have essentially identical structures and charge distributions (outside of the 4f-electron shell). The results obtained in the present study also yield k_q(Tb*–Co) values larger than k_q(Eu*–Co) values for all of the CoNDP and CoNTP quenchers except CoADP. The ratio of k_q(Tb*–Co) to k_q(Eu*–Co) is 0.86 for CoADP, 1.03 for CoATP, and >1.84 for the other seven quenchers (see the data in Table I and Figure 4). The k_q values for Eu*–CoADP and Eu*–CoATP quenching are higher than expected, and the reasons for this are unclear.

In the studies reported here, variations in k_q values *within* the respective k_q(Eu*–Co) and k_q(Tb*–Co) data sets reflect sensitivity to the base moiety and the di- or triphosphate composition of the nucleotide ligand *and* to quencher charge. Earlier (see Results section) we discussed differences between CoNDP and CoNTP quenching data in terms of quencher charge effects, but it is likely that these differences also reflect structural effects associated with the di- vs triphosphate moieties of the respective quencher complexes. The CoNDP complexes are smaller (and possibly less structurally flexible) than their CoNTP counterparts, and this might enhance energy-transfer rates by allowing the Ln* and Co metal centers to get closer together in the Ln*–Co precursor complexes. If this speculation is valid, then both charge and structural effects would make CoNDP complexes more effective quenchers than their CoNTP counterparts.

Variations in k_q values within the Eu*–CoNTP and Tb*–CoNTP data sets show, qualitatively, the same trends with respect to the relative effectiveness of different CoNTP complexes as quenchers. The order of effectiveness among the *purine* CoNTP complexes is CoATP ≫ CoGTP > CoITP, and the order of effectiveness among the *pyrimidine* CoNTP complexes is CoCTP > CoUTP ≈ CoTTP. Among *all* the CoNTP complexes, CoATP is by far the most effective quencher and CoITP is the least effective (see Table I and Figure 4). These nucleotide-base-dependent variations in k_q indicate significant structural differences among the CoNTP complexes, and these structural differences can be reflected in both the K_a and k_e factors of eq 31. Nucleotide ligand effects on the k_e rate constants must necessarily involve perturbations of the $3d^6$ electronic-state structure (and 3d–3d transition properties) of the Co(III) metal center since the acceptor states in Ln*-to-Co energy-transfer processes derive from the $3d^6$ electronic configuration of Co(III).[2] Among the CoNTP complexes examined in this study, it is likely that these perturbations would be modulated in large part by interactions between the nucleoside base moiety and ligand atoms (or groups) coordinated directly to Co(III). The K_a factor of eq 31 would also be sensitive to interactions between the base moiety and atoms within the $Co(NH_3)_4$(phosphate) coordination unit since these interactions would play a significant role in determining the relative shapes, sizes, and charge distributions of CoNTP structures.

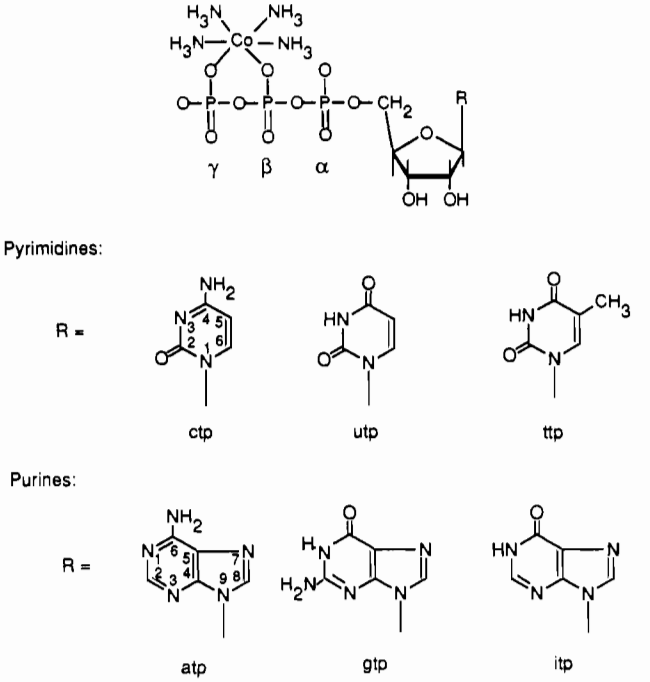

Figure 5. Structural representations of the $Co(NH_3)_4$(nucleotide triphosphate) complexes used in this study. Note that for the ttp structure the sugar moiety is a deoxyribose, rather than the ribose structure shown.

It is interesting to note that, among the CoNTP complexes, the two most effective quenchers are CoATP and CoCTP. In CoATP, the purine ring has an NH_2 substituent at the C-6 carbon atom, which is located diagonally across the ring from the glycosidic linkage at the N-9 nitrogen atom (see Figure 5 for structural representations). In CoCTP, the pyrimidine ring has an NH_2 substituent at the C-4 carbon atom, which is directly across the ring from the glycosidic linkage at the N-3 nitrogen atom. In CoGTP and CoITP, the C-6 carbon atom of the purine ring has a carbonyl oxygen atom substituent, and in CoUTP and CoTTP, the C-4 carbon atom of the pyrimidine ring has a carbonyl oxygen atom substituent. On the basis of these structure considerations, one can speculate that amino vs oxygen substitution at the purine C-6 or pyrimidine C-4 position has a significant influence on the electronic and/or structural factors that determine quencher effectiveness. The differentiating influence of amino vs oxygen substitution at the purine C-6 position is most apparent in the k_q data for CoATP vs CoITP. The purine bases in these systems are identical except for the C-6 substituent, but the ratio of k_q(Ln*–CoATP) to k_q(Ln*–CoITP) is *2.5* for Tb* quenching and *4.7* for Eu* quenching.

The enantiodifferential quenching results obtained in this study are rather remarkable in several respects. First, the degree of enantioselectivity reflected in the $|E_q|$ values for most of the Ln*–Q systems is somewhat higher than might be expected for the types of quencher complexes used in this study. These complexes were not present in solution as resolved optical isomers, but rather as mixtures of diastereomeric structures in which the only "resolved" elements of chirality lie outside the $Co(NH_3)_4$(phosphate) coordination unit. Second, the relative magnitudes and signs of the E_q values show that both the *degree* and *sense* of chiral discrimination (in ΛLn*–Q vs ΔLn*–Q quenching) are influenced decisively by the purine or pyrimidine base moiety of the nucleotide ligand. Considered as isolated structural entities, the base moieties are inherently achiral. However, in the CoNDP and CoNTP complexes, their location and orientation *relative* to the other structural subunits may contribute to the overall configurational chirality of a complex and thereby influence the enantioselective quenching properties of the complex. Therefore, one may anticipate that structural differences between the various CoNDP and CoNTP complexes will be reflected in the E_q parameter values. Perhaps the most striking feature of our enantioselective quenching results is the variation in the relative *sign* of E_q. Recall

that E_q values of opposite sign correspond to opposite preferences for ΛLn* vs ΔLn* quenching *and* therefore a change in the *sense* of chiral discriminatory interactions between the luminophore and quencher species. This suggests that changes in the sign of E_q with quencher variation must correspond to major structural differences between the quenchers. However, chiral discriminatory interactions and their relationship to structure are subtle (and poorly understood), so this suggestion must be considered with some circumspection.

In all of our previous studies of enantioselective quenching kinetics, the quenchers were chiral transition-metal complexes that could be prepared and studied as pure enantiomers. These complexes have tris(bidentate) chelate structures, of either D_3 or pseudo-D_3 (actual C_2) symmetry, in which configurational chirality about the metal center is determined by the spatial disposition of the three chelate rings. Resolved enantiomers of these complexes have rigid and well-defined stereochemical structures (of known absolute configuration about the metal ion), and they exhibit strong circular dichroism in electronic transitions that involve d orbitals of the metal ion (e.g., d–d or d ↔ ligand charge-transfer transitions). This implies chirality in the wave functions of electronic states that serve as acceptor states in the Ln*-to-Q energy-transfer processes. Differential quenching of ΛLn* and ΔLn* luminophores by an enantiomerically *pure* population of ΛQ quencher complexes may be analyzed entirely in terms of differential *homochiral* (ΛLn*–ΛQ) vs *heterochiral* (ΔLn*–ΛQ) interactions. Furthermore, if the mechanistic model of ref 4 is adopted, it may be assumed that these differential (chiral discriminatory) interactions are subsumed in the K_a^Λ, K_a^Δ, k_e^Λ, and k_e^Δ parameters of eqs 32–35. Chiral discrimination in the formation and dissociation of homochiral vs heterochiral encounter (or precursor) complexes is reflected in the sign and magnitude of $K_a^\Lambda - K_a^\Delta$, and chiral discrimination in ΛLn*-to-ΛQ vs ΔLn*-to-ΛQ energy-transfer processes is reflected in the sign and magnitude of $k_e^\Lambda - k_e^\Delta$. The relative contributions of these two types of chiral discrimination to enantioselective quenching are difficult to evaluate, but some progress has been made in identifying systems where the contributions can be *qualitatively* distinguished.

The CoNDP and CoNTP complexes employed as quenchers in the present study exist as mixtures of diastereomeric structures that are devoid of symmetry. The six-membered chelate ring of the $Co(NH_3)_4$(phosphate) coordination unit contains an asymmetric phosphorus atom, and permutation of the two exocyclic substituents on this phosphorus atom generates two stereoisomers that differ with respect to (1) configurational chirality about the asymmetric phosphorus atom and (2) conformational chirality within the chelate ring. Cornelius and Cleland have shown that when these two stereoisomers are separated (for the CoADP and CoATP complexes), they exhibit substantial circular dichroism, of opposite sign, in the d–d electronic transitions of Co(III).[8c] On the other hand, samples that contain unseparated mixtures of these stereoisomers exhibit only very weak d–d circular dichroism. These stereoisomers are not structural isomers, but the d electrons of Co(III) effectively view them as enantiomers. In the present study, we used unseparated mixtures of these stereoisomers (denoted as RQ and SQ in the Theory and Measurement Methodology section), and the quencher complexes may be considered as quasi-racemic mixtures with respect to structural chirality within the $Co(NH_3)_4$(phosphate) coordination units. This implies that the chiral discriminatory interactions responsible for enantioselective quenching must derive from structural chirality associated with the nucleoside part of the nucleotide ligand in CoNDP and CoNTP complexes. The asymmetric carbon atoms in the sugar moiety certainly contribute to the structural chirality of the nucleoside, but structural chirality associated with the *overall* spatial arrangement (including relative positions and orientations) of the sugar *and* base moieties around the $Co(NH_3)_4$(phosphate) coordination unit appears to play the dominant role in ΛLn*–Q vs ΔLn*–Q chiral recognition processes. This is indicated by the dramatic variation of E_q values with changes in the nucleoside base (vide supra).

On the basis of the structural considerations discussed above, one can speculate that enantioselective quenching by the CoNDP and CoNTP complexes is governed largely by the relative shapes, sizes, internal geometries, and electrostatic interactive strengths of ΛLn*–Q vs ΔLn*–Q encounter (or precursor) complexes rather than by chirality inherent in the donor and acceptor states that participate in electronic energy transfer. All of these governing factors will be reflected in the K_a^Λ and K_a^Δ parameters of eqs 32–35, and the size and internal geometry factors could also be reflected in the k_e^Λ and k_e^Δ rate parameters.[4]

Finally, we comment on two assumptions that are implicit in all of our discussion up to this point. The first assumption is that quenching occurs via electronic energy transfer between donor states localized on the lanthanide ion of the $Tb(dpa)_3^{3-}$ and $Eu(dpa)_3^{3-}$ luminophores and acceptor states localized on the cobalt ion of the CoNDP or CoNTP quencher complexes. The second assumption is that Ln*-to-Co energy transfer occurs only when the luminophore and quencher species are in contact or near-contact with each other (as in solution encounter complexes).

The *resonance* conditions for electronic (or vibronic) energy-transfer processes are satisfied for both the Tb*–Co and Eu*–Co systems examined in this study. It is not possible to make conclusive statements about the mechanistic details of the energy-transfer processes, but some general comments are in order. First, we note that all of the resonant emissive and absorptive transitions in the Eu*–Co systems have very low oscillator strengths, and it is very unlikely that multipole–multipole interactions between Eu* and Co transition densities make any significant contributions to Eu* → Co energy transfer. This energy transfer is probably dominated by an electron-exchange mechanism.[2,4] On the other hand, several of the Tb* emissive transitions (including the most intense one, $^7F_5 \leftarrow {}^5D_4$) overlap the lowest-energy *spin-allowed* d–d absorption band of Co(III), and it is possible that a multipole–multipole interaction mechanism may contribute significantly (*or* predominantly) to Tb* → Co energy transfer. However, no matter which mechanism is considered to be the dominant one (in Eu* → Co *or* Tb* → Co energy transfer), one may predict short critical transfer distances *and* the necessity of having the Ln* and Co systems in close contact prior to energy transfer. This prediction is based on the compact (or "buried") nature of the 4f-electron distributions in lanthanide ions and on the inherently low oscillator strengths of lanthanide 4f–4f transitions. The 4f(Ln*)–3d(Co) orbital overlap required in the electron-exchange mechanism can only occur at short Ln*···Co separation distances, and the 4f–4f multipolar transition amplitudes required in the multipole–multipole interaction mechanism can induce 3d–3d excitations on Co only at short Ln*···Co separation distances. In our previous studies of Eu*–Co and Tb*–Co systems,[2,4,5] we found that the quenching rate constants (k_q) decrease with increasing ligand size for Co(III) complexes that are otherwise similar (with respect to net charge, ligand donor atoms, and chelate ring distribution). This implies that the quenching rates are governed (at least in part) by Ln*···Co separation distances dictated by *contact* interactions.

Magnesium(II) analogues of the CoNTP complexes *do not* quench Eu* or Tb* luminescence,[5] whereas rhodium(III) analogues of these complexes *do* function as quenchers.[17] These results show that Rh(III), like Co(III), has suitable acceptor states for Ln*-to-Q electronic energy transfer, whereas Mg(II) does not. These results also support our assumption that the ligands of the $Co(NH_3)_4$(nucleotide) complexes do not participate directly in the electronic energy-transfer part of the quenching processes. However, the ligands can exert an influence on both the K_a and k_e parameters of eq 31 by regulating the formation, dissociation, and structural properties of Ln*–Q precursor complexes, and by perturbing the wave functions and energies of the Co(III) acceptor levels.[4]

Conclusion

The enantioselective quenching results obtained in this study give a striking demonstration of chiral discrimination in dynamic intermolecular interaction processes. Relatively small concen-

trations of dissymmetric quencher molecules (CoNDP or CoNTP) in solution with a racemic excited-state population of luminophores (ΛLn* and ΔLn*) can produce substantial enantiomeric excess in the Ln* population via enantiodifferential rate processes for ΛLn* vs ΔLn* quenching. Evidence for the creation of an enantiomeric excess in the Ln* population is provided by circularly polarized luminescence measurements, and the rate of formation of this enantiomeric excess can be determined from time-resolved emission dissymmetry (g_{em}) measurements. Examples of CPL spectra generated by enantioselective quenching in Tb*-CoATP and Tb*-CoGTP systems are shown in Figures 2 and 3, and the values determined for several enantioselective quenching parameters (e.g., k_{bq} and E_q) are summarized in Table I.

The enantioselective quenching results exhibit a number of interesting features, and we have identified and discussed these features in earlier parts of the paper. The most striking features are those reflected in the relative signs and magnitudes of E_q values determined for the six CoNTP and three CoNDP quencher complexes (see Table I and Figure 4). As illustrations, consider the following results for Tb* quenching: (a) CoATP quenches one enantiomer of Tb* 32% more efficiently than the other and CoGTP quenches one enantiomer of Tb* 16% more efficiently than the other, but CoATP and CoGTP have *opposite* enantiomeric preferences; (b) CoGTP and CoGDP show essentially identical quenching behavior, whereas CoATP and CoADP differ with respect to enantiomeric preference *and* the degree of enantioselective quenching. Interpretation of these results in terms of detailed structural or mechanistic models of intermolecular chiral discriminatory interactions is beyond the scope of the present work. Given the structural complexities of the systems and the subtleties of chiral discriminatory interactions, detailed interpretation of the results is a rather daunting task. However, this task will become easier as more enantioselective quenching studies are carried out on additional, structurally related systems. In our laboratory, we have begun a systematic study of *bidentate* Rh(H_2O)$_4$(nucleotide) and *tridentate* Rh(H_2O)$_3$(nucleotide) complexes as enantioselective quenchers of Eu* and Tb* luminescence. These complexes provide additional variations in stereochemical structure, and the replacement of Co(III) with Rh(III) provides an opportunity for examining how quenching is influenced by the electronic-state structure of the quencher metal.

Acknowledgment. This work was supported by grants from the National Science Foundation (CHE-8820180 to F.S.R.), the National Institutes of Health (DK 19419 to C.M.G.), and the Muscular Dystrophy Association of America.

Registry No. Tb(dpa)$_3^{3-}$, 38682-37-0; Eu(dpa)$_3^{3-}$, 38721-36-7; [Co(NH_3)$_4$(adp)], 63937-09-7; [Co(NH_3)$_4$(gdp)], 113903-18-7; [Co(NH_3)$_4$(idp)], 141345-92-8; [Co(NH_3)$_4$(atp)]$^-$, 63915-28-6; [Co(NH_3)$_4$(gtp)]$^-$, 141345-93-9; [Co(NH_3)$_4$(itp)]$^-$, 141345-94-0; [Co(NH_3)$_4$(ctp)]$^-$, 141345-95-1; [Co(NH_3)$_4$(utp)]$^-$, 141345-96-2; [Co(NH_3)$_4$(ttp)]$^-$, 141374-98-3.

Contribution from the Department of Chemistry, University of California at Santa Barbara, Santa Barbara, California 93106

Unusual Behavior of 5,10,15,20-Tetraphenylporphine Diacid toward Oxygen Bronsted Bases

Rafik Karaman and Thomas C. Bruice*

Received June 19, 1991

Acid-base properties of 5,10,15,20-tetraphenylporphine diacid salts ($H_4TPP^{2+}(X^-)_2$) in the presence of neutral oxygen Bronsted bases have been studied in chloroform and nitrobenzene by visible and ^{1}H-NMR spectroscopy. The acid strength and the conformation of $H_4TPP^{2+}(X^-)_2$ are largely determined by the size and the nature of the counterion X^-. Localized negatively charged counterions, such as Cl^-, stabilize the protonated porphyrin by forming a strong tight-contact pair with the cationic porphyrin moiety, whereas delocalized negatively charged counterions, such as ClO_4^-, form a weak tight-contact pair and hence destabilize the porphyrin diacid by increasing its acidity. Defining the acidity by the concentration of Bronsted base required for half-neutralization of H_4TPP^{2+}(C50%), we find the acidity of $H_4TPP^{2+}(X^-)_2$ salts to be linearly correlated with both the size of the counteranion (r) and the chemical shift of the NH pyrrolic resonance of the porphyrin core (CS). Furthermore, the correlations of the acidity of $H_4TPP^{2+}(X^-)_2$ both with the pK_a of the neutral oxygen base solvents, measured in sulfuric acid-water solutions, and with the donicity number (D) of the oxygen Bronsted bases suggest that the mechanism of deprotonation of $H_4TPP^{2+}(X^-)_2$ is dependent upon both the basicity and the solvation power (donicity) of the Bronsted neutral oxygen base solvents.

Introduction

Porphyrins and metalloporphyrins have attracted the interests of chemists and biochemists alike, and their physical, chemical, and biological properties have been extensively studied over the last 50 years.[1] Little is known, however, about the chemistry of their mono- and diprotonated species, namely porphyrin acids (eqs 1 and 2). The X-ray crystal structures, as well as UV/vis and

$$H_2TPP \xrightarrow{H^+} H_3TPP^+ \quad (1)$$

$$H_3TPP^+ \xrightarrow{H^+} H_4TPP^{2+} \quad (2)$$

IR spectra, of a few porphine diacids[2] (5,10,15,20-tetra-4-pyridylporphine and 5,10,15,20-tetraphenylporphine[2a]) have been reported, as has the structure of a porphine monoacid salt (octaethylporphinium monoacid triiodide[2b]). It has been shown that the protonated octaethylporphyrin cation and triiodide counteranion ($(OEPH_4)^{2+}(I_3^-)_2$) are strongly associated through hydrogen bonding in chloroform, whereas in methanol the diprotonated species dissociates into monoprotonated porphyrin and HI.[2c] Our interest in the porphine diacids stems from observations in this laboratory that their treatment with the common organic solvents DMSO, DMF, Et_2O, etc. leads to their deprotonation.[3] Though

(1) (a) Dolphin, D., Ed. *The Porphyrins*; Academic Press: New York, 1979. (b) Smith, K. M., Ed. *Porphyrins and Metalloporphyrins*; Elsevier Scientific Publishing Co.: Amsterdam, 1975.

(2) (a) Stone, A.; Fleischer, E. B. *J. Am. Chem. Soc.* **1968**, *90*, 2735. (b) Hirayama, N.; Takenaka, A.; Sasada, Y. *J. Chem. Soc., Chem. Commun.* **1974**, 330. (c) Ogoshi, H.; Watanabe, E.; Yoshida, Z. *Tetrahedron* **1973**, *29*, 3241.

(3) The same phenomenon was observed for dimeric porphyrins: (a) Bookser, B. C.; Bruice, T. C. *J. Am. Chem. Soc.* **1991**, *113*, 428. (b) Karaman, R.; Bruice, T. C. *J. Org. Chem.* **1991**, *56*, 3470-3472.

0020-1669/92/1331-2455$03.00/0